

# Topology optimization for finding shell structures manufactured by deep drawing

R. Dienemann, A. Schumacher and S. Fiebig

**Abstract** This paper presents a new approach for optimizing shell structures considering their mid surface design including cut-outs. Therefore we introduced a manufacturing constraint to the 3D topology optimization based on the density method in order to receive an optimized structure without undercuts and with a constant wall thickness, so that these structures can be manufactured by deep drawing in one step. It is shown that introducing cut-outs while increasing the shell thickness can improve the performance of shell structures considering their stiffness at a constant mass.

**Keywords** topology optimization, sheet metals, deep drawing, manufacturing constraint, thin walled structures

## 1 Introduction

Applying 3D topology optimization to continuum structures for minimum compliance or minimum stress at minimum mass, usually results in complex structures with undercuts and a very complicated distribution of the structure's thickness. Manufacturing those structures is often only possible by joining many components or by 3D printing.

By introducing existing manufacturing constraints and an integrated casting simulation, producible casting parts can be obtained by the 3D topology optimization (Harzheim et al 2006, Xia et al. 2009, Guest and Zhu 2012, Allaire et al. 2013, Franke et al. 2015).

Considering the mass production costs, it is often more reasonable to manufacture sheet metal parts by deep drawing. Furthermore deep drawing is a manufacturing process, which allows the forming of very thin walls. In contrast to casting parts, the material properties of deep drawn blanks are better, because the initial blank has less defects and the yield strength increases during the manufacturing process due to the material hardening.

In order to obtain structures from the topology optimization without undercuts and with a constant wall thickness, we implemented a manufacturing constraint to the 3D topology optimization based on the density method. Thereby the variety of possible shapes of the mid surface is flexible and not dependent on a predefined parametrization. By using a topology optimization approach, cut-outs can be realized during the optimization, in contrast to a shape optimization approach, which is often used for shell optimizations.

In this paper topology optimized deep drawing structures are compared with optimized topologies without manufacturing constraints due to their design and performance. Furthermore it is investigated how a thinning or thickening of the structure affects the optimization result.

Research on the optimization of shell structures has been done in mechanical engineering, but also in civil engineering and architecture, e.g. considering roof structures.

Ansola et al. (2002) combined shape and topology optimization for shell structures. A combination of CAD-parameters for the mid surface description and the SIMP-algorithm for the identification of optimal cut-outs is proposed. Their optimization algorithm performs sequentially the shape optimization of the mid surface and afterwards the topology optimization. Hassani et al. (2013) modified this approach by doing a simultaneous shape and topology optimization. The shape of the mid surface is parametrized by the control points of NURBS. Thereby the node coordinates of the shell mesh are controlled and also the shape optimization takes place in the Finite Element Model. Both methods highly depend on the parametrization of the mid surface.

Bletzinger and Ramm (2014) perform shape optimization based on node coordinates as design variables. They cope with large shape modifications without mesh distortion by applying a sufficiently large filter radius.

In topography optimization nodes can be moved in the normal direction to the shell surface in order to generate reinforcement patterns of beads (e.g. Altair OptiStruct). Thereby often an artificial stiffening occurs due to the mesh distortion. Cut-outs are not addressed with the topography approach.

Only few works try to use the continuum approach to optimize shell structures. The density method is used by Lochner-Altdinger and Schumacher (2014) whereby isosurfaces of the element densities are extracted as possible mid surfaces.

An initial approach for a stamping constraint has been implemented in Altair OptiStruct, which introduces a lot of constraints to the optimization task in order not to exceed a given sum of element densities in the punch direction (Zhou et al. 2011).

The work presented in this paper contributes to the Volkswagen LEOPARD – Lightweight Optimization and Robust Design (Fiebig et al. 2015). This tool also enables advanced topology

optimization for casting parts with integrated casting simulation, multimaterial optimization (Falkenberg et al. 2015) and addresses acoustic responses (Bertsch et al. 2008).

The paper is organized as follows. Section 2 gives a brief introduction to the deep drawing process. The used continuum topology optimization approach is described in section 3. In order to use the continuum approach for the optimization of shells, manufacturing constraints have to be implemented. These manufacturing constraints allow the approximation of shells as thin walled continuum structures, while maintaining the optimization approach. The optimization problem and the basic idea of the manufacturing constraints are outlined in section 4. In section 5 the implementation of the manufacturing constraint and the solution of a convergence issue is discussed. Various examples are shown in section 6 and 7, whereby the performance of the optimization method is examined.

## 2 A brief introduction to the deep drawing process

Deep drawing is a manufacturing process that is used extensively in the forming of sheet metals (see Fig. 1). Thereby an initially flat sheet metal (blank) with a constant wall thickness is formed by a moving punch and a fixed die. Usually a blank holder is applied to restrain the sheet metal outside the area under the punch in order to impose a stress state dominated by tension. Thus a buckling of the sheet metal (wrinkling) during the manufacturing due to compressive stresses is avoided.

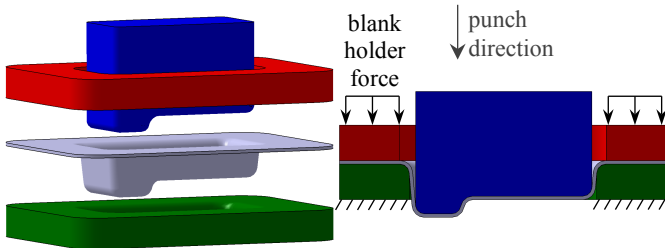


**Fig. 1** Deep Drawing: exploded view and cross section with formed sheet metal (grey), punch (blue), die (green) and blank holder (red)



**Fig. 2** Sheet metal cross section

In Fig. 2b) a modified contour of the sheet metal is shown. This contour cannot be deep drawn in one step because of the undercut in punch direction highlighted with the red shading. Our manufacturing constraint also covers similar manufacturing processes like stretch-forming or embossing. Cut-outs can be introduced before or after the deep drawing process, but a deep drawing with cut-outs will more likely fail due to tearing (fracture of the sheet metal).

## 3 Density Method

Our new approach is inspired by the homogenization method (Bendsøe 1989). The popular material interpolation approach Solid Isotropic Material with Penalization (SIMP) was derived from the homogenization method and is applied in our approach on a voxel mesh consisting of 8-node linear finite elements. SIMP introduces material with the artificial density  $0 < x_{\min} \leq x_i \leq 1$  and Young's modulus  $E_i$  in element  $i$  (see equation 1).  $E_0$  is the Young's modulus of the solid material. By increasing the penalty exponent  $s$  over 1.0, intermediate densities are penalized and thereby the optimized design rather converges to a black&white design, which means that fewer elements with intermediate density exist in the optimized result.

$$E_i = x_i^s E_0 \quad (1)$$

By using a gradient based algorithm, our approach is suitable for linear or slightly nonlinear load cases. Every objective function or constraint can be used efficiently, if their sensitivities can be calculated analytically. We implemented criteria for volume, compliance, eigenfrequency, nodal displacement and a global stress criterion based on Le et al. (2010).

To generate a well-posed topology optimization problem, we use a sensitivity filter (Sigmund and Petersson 1998) for the examples in this paper. The filter's regularization leads to an overcoming of local minima due to checkboards. The filter also imposes a minimum length scale. The filtered sensitivity of element  $i$  is defined by the weighted average of the sensitivities of elements  $j$ , which are inside the neighborhood of element  $i$  defined by the filter radius  $r$ .

$$\frac{\tilde{\partial f}}{\partial x_i} = \frac{\sum_j w_j x_j \frac{\partial f}{\partial x_j}}{\sum_j w_j x_j} \quad (2)$$

where  $\frac{\partial f}{\partial x_j}$  are the element's sensitivities of the objective or

constraint function  $f$ ,  $\frac{\tilde{\partial f}}{\partial x_i}$  are the filtered sensitivities and

$w_j = \max(r - \text{dist}(i, j), 0)$  are the weighting factors with the distance between the element mid points  $\text{dist}(i, j)$ .

As optimization algorithms we implemented the Optimality Criterion and the Method of Moving Asymptotes (MMA, Svanberg 1987) together with the dual optimization method (Fleury 1989).

#### 4 Aim of topology optimization for deep drawable sheet metals

With the presented approach the shape of the mid surface (including beads) shall be optimized as well as the topology of the mid surface by introducing cut-outs. Thereby deep drawing of the optimized structure in one step should be ensured.

The following optimization problem is solved

$$\begin{aligned} \min_x : \text{Compliance } c(\mathbf{u}(\mathbf{x})) &= 0.5 \mathbf{f} \cdot \mathbf{u} \\ \text{subject to: } \frac{V(\mathbf{x})}{V_0} &= \frac{\sum_{i=1}^N x_i}{N} \leq \bar{v} \\ \mathbf{K}(\mathbf{x})\mathbf{u} &= \mathbf{f} \end{aligned}$$

with manufacturing constraints

- constant wall thickness  $b \approx \bar{b}$
- no undercuts in punch direction  $\mathbf{h}$
- no ribs

Input parameters are the maximum volume fraction  $\bar{v}$ , the desired wall thickness  $\bar{b}$  and the punch direction  $\mathbf{h}$ .  $\mathbf{f}$  and  $\mathbf{u}$  are the global load and displacement vector,  $\mathbf{K}$  is the global stiffness matrix. The volume fraction is calculated by the filled

volume  $V(\mathbf{x}) = \sum_{i=1}^N x_i \cdot V_{i0}$  divided by the volume of the design space  $V_0$ .  $N$  is the number of design elements and  $V_{i0}$  the volume of the  $i$ -th element, which is the same for every element considering the voxel discretization.

In order to ensure a minimum thickness a common sensitivity filter (equation 2) is used, whereby the filter radius should be larger than half the desired wall thickness. The maximum wall thickness and the avoiding of undercuts and ribs is managed by a new manufacturing constraint.

Some geometrical requirements for deep drawable sheet metals like draw radii and draw bead height are not addressed in this paper. Additionally there are other important restrictions regarding the manufacturing process, which are not considered, because therefore an integrated manufacturing simulation is required. Worth noting are the avoiding of tearings and wrinkles of the shell structure, consideration of hardening and thickness reduction in the deep drawing process (see Boljanovic 2014, Dienemann 2016).

#### 5 New approach – Penalization of the objective’s sensitivities far away from the mid surface

The manufacturing constraints from section 4 can be achieved by modifying the sensitivities of the objective function with penalization functions. An increase of the element densities is only allowed near the current mid surface. Thus the mid surface can move according to the sensitivities.

#### 5.1 Calculation of the mid surface

In Fig. 3 the procedure of deriving the mid surface from the voxel mesh is shown on an exemplary cross section. The user has to define the punch direction in the input deck. This is the direction of the columns, in which the mesh is divided. They have the same width  $w$ . The mid surface can be found by calculating the average of the element coordinates in the punch direction  $\xi_i$  weighted with the element densities  $x_i$ . Therefore the midpoint of each column is calculated by

$$\xi_m = \frac{\sum \xi_i \cdot x_i}{\sum x_i} \quad (3)$$

For one exemplary column the coordinates  $\xi_i$  are marked as grey arrows. The midpoint of each element decides to which column the element belongs. The connection of all midpoints with distance  $\xi_m$  represents the mid surface.

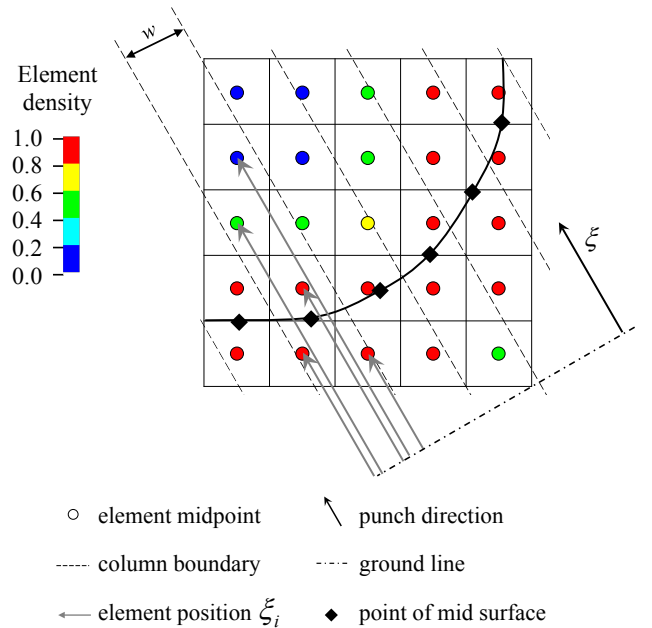


Fig. 3 Calculation of mid surface

As an example a density distribution from an optimization without manufacturing constraint is used as initial design: In a column we have  $\xi_i = [1 \ 2 \ 3 \ 4 \ 5 \ 6 \ 7]$  and  $x_i = [1 \ 1 \ 0 \ 0 \ 1 \ 1]$ . This represents an undercut because of a density concentration at the bottom and the top of the column. The mid surface point is calculated according to equation 3 as  $\xi_m = 4$ . Thus the initial mid surface is located at the void of the initial density distribution. In the following iterations the undercut vanishes and the mid surface point can move continuously towards an improved position.

## 5.2 Penalization of objective's sensitivities

The objective's sensitivities far away from the mid surface are penalized in order to receive a thin walled structure. Therefore the objective's sensitivities are multiplied with the penalty factor  $P_i$

$$P_i = \frac{1 + \exp(-l \cdot a)}{1 + \exp(2a/b \cdot (d_i - l))} \quad (4)$$

with the abbreviation  $l = \ln(-2 + \exp(a \cdot b/2))/a$ ,

which depends on the distance  $d_i$  (unit: element edge lengths) between the midpoint of element  $i$  and the mid surface.

The parameter  $b$  is the user defined desired wall thickness (unit: element edge lengths),  $a$  describes the discreteness of the penalty function (see Fig. 4).

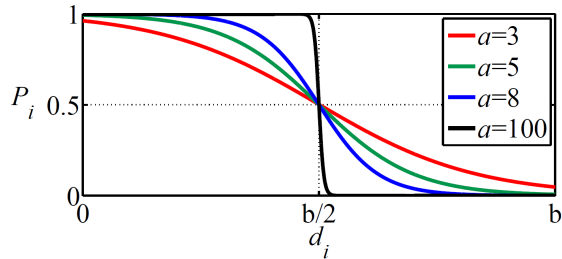


Fig. 4 Examples of penalty functions

A larger  $a$  ensures that the shell thickness does not exceed  $b$ , but slows down the convergence rate. The penalization factor is normalized  $P_i \in ]0,1[$ , in order to maintain the sensitivities near the mid surface unmodified and to scale the sensitivities far away from the mid surface to zero (for the objective function compliance, which is used in the current work).

For minimization problems a penalization means an increase of the objective's sensitivities. For objective functions with negative sensitivities (e.g. compliance), the absolute value of these sensitivities has to be reduced, therefore the penalty factor has to be smaller than one, consequently we multiply the objective's sensitivities with  $P_i$ . If the objective's sensitivities are positive (e.g. volume), then the penalty factor has to be larger than one, so we use the reciprocal of  $P_i$ .

Because the sensitivities of eigenfrequencies, stress criteria or nodal displacements do not have a constant sign, they cannot be used as objective, but as constraint function.

This approach prescribes the maximum wall thickness and avoids undercuts. Also ribs as thin walled stiffening structures, which are perpendicular to a bended basic structure, are avoided. Without undercuts, ribs could only occur with their height dimension exactly in punch direction. Our approach allows only a thin extension in punch direction, so that ribs cannot occur.

## 5.3 Convergence issues

The movement of the mid surface at a constant wall thickness results in a local accumulation of intermediate dense elements. This is shown by Fig. 5. Even if a movement of the mid surface towards the force level would improve the objective function compliance, the stiffness of the structure temporarily decreases due to the lower stiffness of elements with penalized intermediate density (image at the right, see Table 1).

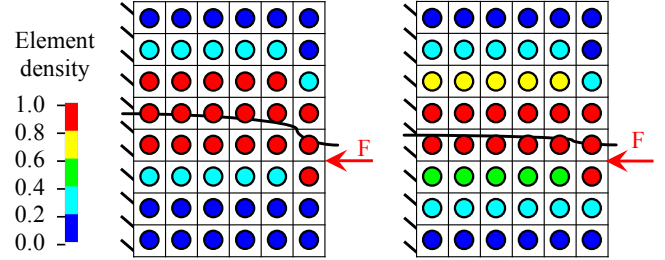


Fig. 5 Movement of mid surface - density distributions, left: example 1, right: example 2

Table 1 Change of compliance due to movement of mid surface

	Normalized compliance, example 1 in Fig. 5	Normalized compliance, example 2 in Fig. 5
$s=1.0$	1.000	0.694
$s=3.0$	1.276	1.279

Hence the combination of

- penalization of sensitivities for a constant wall thickness as described in section 5.2 and
  - the penalization of intermediate densities with  $s > 1$
- results in a lot of local minima (as shown in Fig. 5 – example 1). In order to overcome local minima with poor performance, two additional steps are included in the advanced optimization algorithm:

1. The optimization algorithm starts without penalization of intermediate densities (penalty exponent  $s = 1$ ) until a convergence criterion (referred as ‘convergence criterion 2’) is reached. Then the penalty exponent is increased to  $s = 3$  in order to eliminate intermediate densities.
2. The desired wall thickness  $b$  is not fix during the optimization process. If ‘convergence criterion 1’ is reached and the current desired wall thickness  $b_c$  is equal to the final desired wall thickness  $b_f$ , the algorithm increases the desired wall thickness. Due to this increase, elements are accumulated at the side of the shell, where the sensitivities are larger. If convergence criterion 1 is reached and  $b_c > b_f$ , the algorithm decreases the desired wall thickness. Because of the temporary increase of the desired wall thickness, the shell's mid surface can move to an improved design.

## 5.4 Algorithm

Fig. 6 shows the algorithm. All the parts in black letters show the basic algorithm. The grey parts show the start without penalization of intermediate densities, the alternation of the desired wall thickness and the increase of the penalty exponent. These parts have to be added to cope with the convergence issues. Therefore it is called the advanced algorithm.

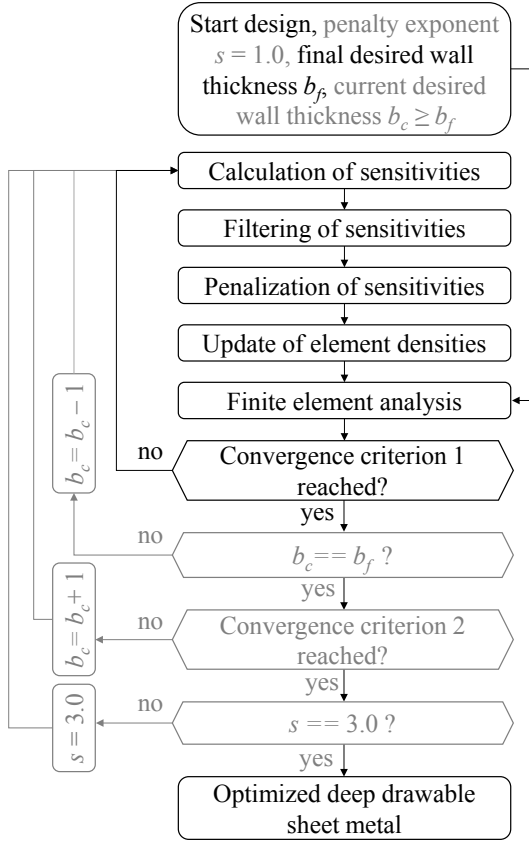


**Fig. 6** Algorithm – black: basic idea, grey: additional effort because of convergence issues

## 5.5 Deactivation of design variables

Due to the nature of thin walled structures most regions of the design space will end up with the minimum element density. In order to save calculation time only elements with a density larger than the minimum density (inner elements) and elements around them within the filter radius (boundary elements) are calculated. Thereby the sensitivities of the inner elements are calculated and filtered correctly.

By using the boundary elements in addition to the inner elements in the optimization algorithm, elements can be reintroduced. This approach is implemented into the Method of Moving Asymptotes by using  $x_{\min}^{MMA} = 0.0$  as lower bound of the active design variables. The boundary elements are calculated with the minimum density although their element density is smaller, in order to obtain a well-conditioned stiffness matrix. Fig. 7 shows the element deactivation during a minimization of the compliance at a maximum volume fraction of 40 % with a filter radius  $r = (1.7 \text{ element edge lengths})$ . As initial design,

the elements at the middle of the design space were chosen. During the optimization, elements at the sides of the fixed end are reintroduced and at the middle of the fixed end are deactivated. The final design is the same as without element deactivation.

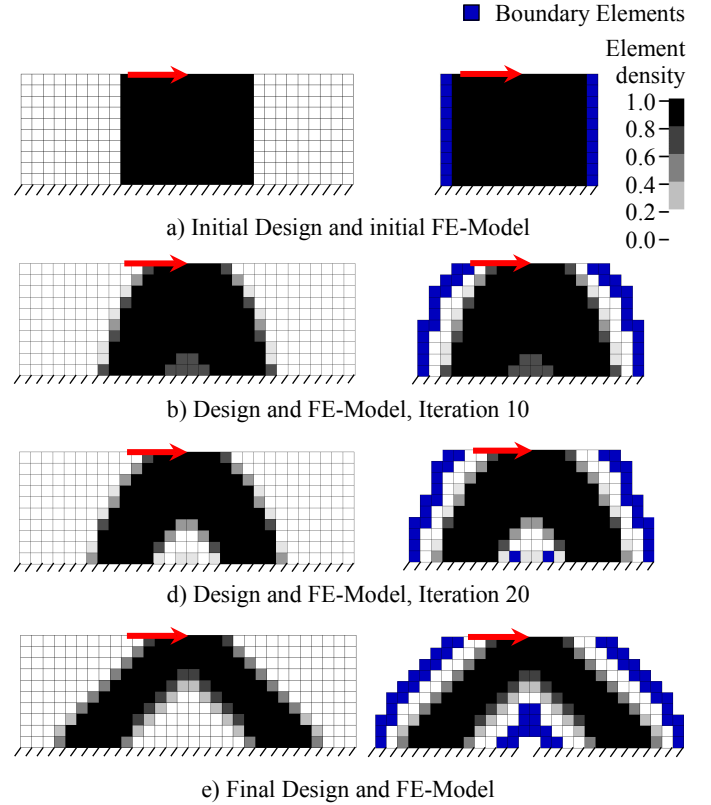


**Fig. 7** Deactivation of design variables

For few boundary conditions or an extensive bearing this concept is reliable. It has to be considered that once a connection to a boundary condition or load gets lost, the connection probably will not be recovered. Therefore it is recommended to use a small minimum density (in this paper:  $x_{\min} = 0.001$ ) and a small initial step width in the optimization algorithm.

## 6 Example 1 – Cantilever Beam

In this section topology optimizations of a cantilever beam (see Fig. 8) are performed with and without manufacturing constraint. The compliance  $c$  is minimized considering a fixed volume fraction of 6.25 % in the design space. Initially about 500 000 Elements with edge length 2.5 mm form the design space. The rear surface of the structure is clamped, at the front bottom edge a line load of  $q=200 \text{ N/mm}$  is applied. The elements at the line load are defined as non-design space. A sensitivity filter (equation 2) with  $r = (1.7 \text{ element edge lengths})$  and a penalty exponent  $s = 3$  are used. The material is steel with Young's Modulus  $E_0 = 210 \text{ GPa}$  and Poisson's ratio  $\nu = 0.3$ . The element densities are initialized uniformly in the design domain. MMA together with a dual optimization algorithm is used for the design update.

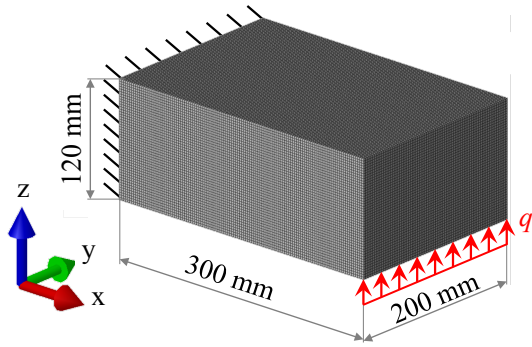


Fig. 8 Cantilever Beam – load case and design space

All optimizations are followed by a final conversion to a black&white design, where a number of elements with the highest densities are recalculated as solid material, so that the volume constraint is satisfied. This postprocessing is an interpretation of the final design, which helps to compare the different optimized structures. As results the black&white designs are evaluated.

All examples are calculated on a computing node with two Intel Xeon E 2650 8-core CPUs and 32 GB memory.

### 6.1 Optimization without manufacturing constraint

Without the manufacturing constraint 215 iterations were necessary to meet the convergence criterion, which is the maximum change of element density per iteration of less than 0.01. The wall-clock time was approximately 7 hours. A compliance of 15.4 Nm is achieved (see Fig. 9).

During the last 180 Iterations less than 80 000 elements were active, which results in a calculation time of 25 s. This is an immense reduction compared to the calculation time with all elements (at the first iterations) with a calculation time of 1200 s. These results were obtained using a direct solver. Using an iterative solver the saving of calculation time is not that excessive.

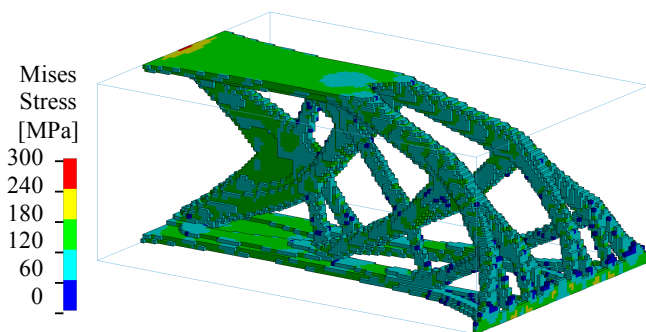


Fig. 9 Optimized Cantilever Beam without manufacturing constraint (black&white design)

### 6.2 Optimization with manufacturing constraint

The same optimization task as in section 6.1 is performed using the manufacturing constraint for thin walled structures. The desired wall thickness is  $b_f = (3 \text{ element edge lengths})$ . This is the thinnest possible wall thickness that allows a sufficiently

accurate representation of a bending stress state with linear volume elements. The punch direction was chosen as  $z$ .

The convergence criterion 1 is

- the improvement of the objective function per iteration of less than 0.1 %
- at a simultaneous
  - maximum change of element density per iteration of less than 0.1
  - or an increase of the objective function.

The convergence criterion 2 is the improvement of the objective function through an alternation of the wall thickness of less than 0.1 %. These criteria are used for all following examples. The penalization parameter for the manufacturing restriction is chosen as  $a = 8$ .

### Basic algorithm

In Fig. 10 the converged structure without alternation of the desired wall thickness and with a constant penalty exponent of  $s = 3.0$  is shown (basic algorithm as shown in black letters in Fig. 6).

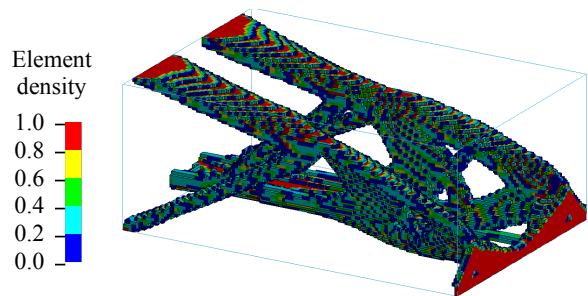


Fig. 10 “Optimized” Cantilever Beam with manufacturing constraint, basic algorithm, thresholded at  $x_i = 0.1$

The optimization converges after 732 iterations and the resulting structure fulfills all geometrical requirements, so it has no undercuts or ribs and a constant wall thickness. But obviously that structure with a compliance of 25.9 Nm can just be a very bad local optimum caused by the penalization of the sensitivities. This shows that additional effort is needed to solve the convergence issues and reduce the number of iterations.

### Advanced algorithm

Fig. 11 shows the history of the objective function value during the optimization with the advanced algorithm. The density plots corresponding to the grey dots can be found in Fig. 12.

As shown in Fig. 11 we start with the desired wall thickness  $b_c = (5 \text{ element edge lengths})$ . This is chosen, because a larger desired wall thickness usually results in a faster movement of the mid surface. During the first iterations the compliance increases because the initial design does not fulfill the manufacturing constraint.

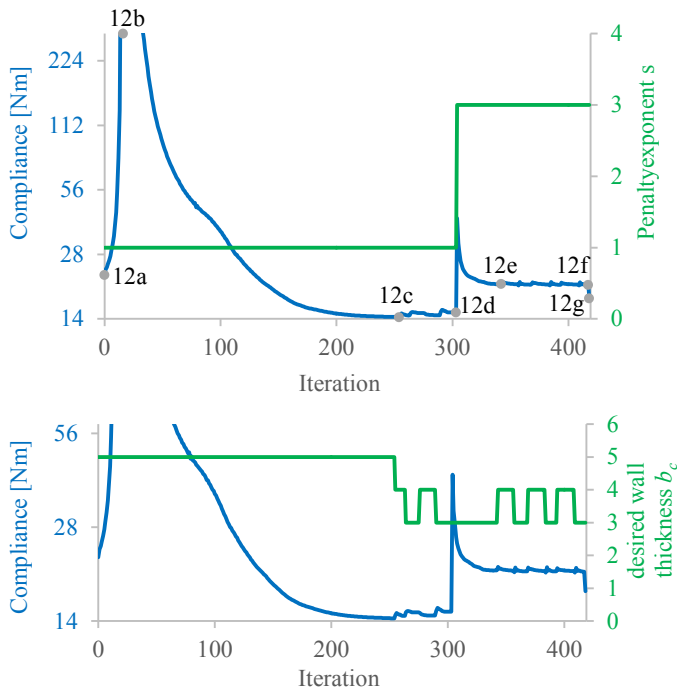


**Fig. 11** Optimization history

From Fig. 11 it can also be seen, that the compliance increases significantly while increasing the penalty exponent. It can be concluded that the structure from Fig. 12d is the best, but because of the penalty exponent  $s=1.0$  the structure consists mainly of intermediate dense elements. This can be interpreted as an optimized shell with variable thickness. In order to obtain a deep drawable sheet metal, a structure with constant wall thickness is required. By increasing the penalty exponent most intermediate dense elements are eliminated, so a shell with constant thickness is achieved and cut-outs are introduced. Due to the alternation of the desired wall thickness (iteration 343-417) the compliance improves by only 1 %, because the mid surface moves slightly from Fig. 12e to Fig. 12f.

In Fig. 13 the final design of the shell structure without intermediate densities using the advanced algorithm from Fig. 6 is shown. This structure reaches a compliance of 17.4 Nm. In comparison to the optimization without manufacturing constraint the compliance is 11 % worse (see Table 2), whereby the manufacturing by deep drawing of an initially flat blank is possible, which is much easier than casting or milling of the optimized structure in Fig. 9.

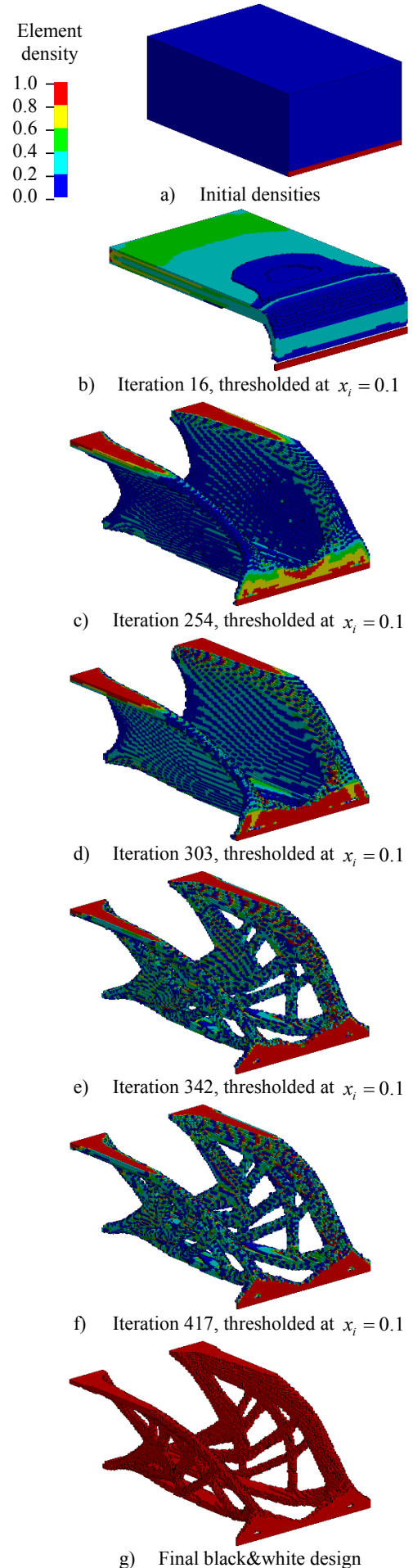


**Fig. 12** Density evolution

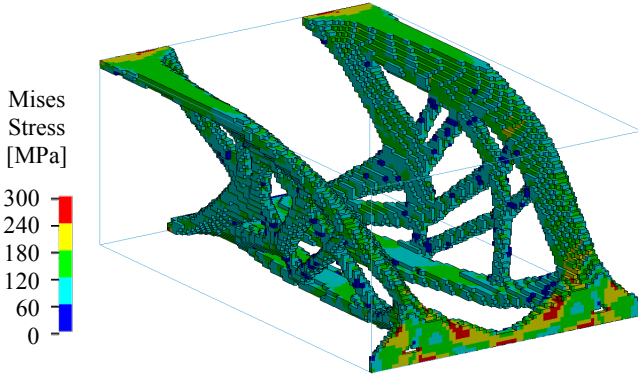


Fig. 13 Optimized Cantilever Beam with manufacturing constraint

Table 2 Results with and without manufacturing constraint

Result	Fig. 9	Fig. 10	Fig. 13
Compliance [Nm]	15.44	25.93	17.46

### 6.3 Structural and mesh refinement

It is investigated how the optimized design changes while refining the mesh. The mesh is refined by splitting one voxel into 8 smaller ones. The finest mesh is calculated with symmetry conditions using half the design space. After each refinement the optimized design of the coarser mesh is used as initial design for the finer mesh. The desired wall thickness is kept constant at  $b_f = (3 \text{ element edge lengths})$  and a filter radius of  $r = (1.7 \text{ element edge lengths})$  is used.

Table 3 and Fig. 14 show that there is a nearly reciprocal relation between the wall thickness and the compliance as well as the mean stress. This is a typical behavior of structures under tension/compression and shows that a stress state dominated by membrane stresses is maintained during the refinement.

Table 3 Structural and mesh refinement

Mesh level	1	2	3
Wall thickness $b_f$ [mm]	7.5	3.75	1.875
Volume fraction [%]	6.25	3.125	1.5625
Elements in design space	460800	3686400	14745600
Iterations needed	417	168	333
Used wall clock time [hours]	10	16	79
Compliance of full model [Nm]	17.46	39.93	79.75

The coarse mesh level needs the most iterations. This is caused by the initial design guess, which is uniform for this optimization. In contrast to that the optimizations with the finer mesh use the optimum of the coarser mesh as initial design guess. Therefore a good mid surface design is already given.

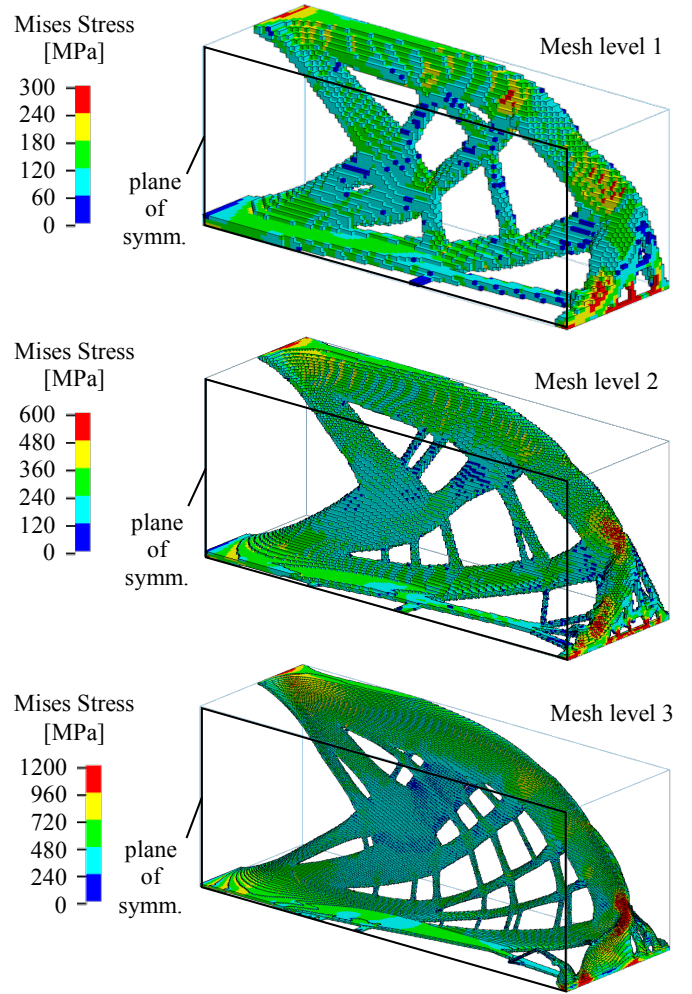


Fig. 14 Optimized Cantilever Beam with refinement – half model

### 6.4 Finding the best wall thickness

By prescribing the volume and the wall thickness, the area of the mid surface is given. Therefore it is investigated which wall thickness is the best for the application example. Mesh level 3 with a volume constraint of 3.125 % is used while different wall thickness are prescribed. All optimizations use the optimized design of mesh level 2, shown in section 6.3, as initial design.

Table 4 gives an overview of the optimization results for different wall thickness.

Table 4 Change of desired wall thickness

Wall thickness $b_f$ [mm]	1.875	2.5	3.125	3.75	4.375
Filter radius $r$ [mm]	1.25	1.667	2.083	2.5	2.917
Iterations needed	225	213	251	224	187
Wall clock time [hours]	97	86	120	132	125
Compliance of half model [Nm]	21.05	21.44	20.10	19.08	18.71

From Fig. 15 it can be seen that by changing the desired wall thickness the optimized designs change from a shell structure with few cut-outs towards a thin framework structure. In this example the compliance of the thickest structure is 12 % better than the compliance of the thinnest one. The tendency towards an improvement of the compliance by introducing cut-outs can be seen. Thereby the wall thickness was increased in order to achieve a constant mass. For all optimization results we have to remark, that the gradient based approach most probably finds local and not global optima.

Sigmund et al. (2015) showed that closed-wall shell structures with variable thickness are stiffer than Michell-like framework structures. The current paper shows that structures with cut-outs are stiffer than closed-wall shell structures considering a constant wall thickness.

In manufacturing, however, the difficulty to deep draw the sheet metal increases with the number of holes. So a compromise between easy manufacturing and stiffness has to be made.

### 6.5 Recalculation with shell elements

Because the accuracy of the voxel mesh results depends on the number of elements across the thickness, the optimized structures are recalculated with shell elements. Fig. 16 and Fig. 17 show the compliance of the optimized voxel structures from Fig. 15 and the corresponding shell results. It can be seen that for all structures there is a loss of performance due to the manual interpretation of the design. A large discrepancy between the shell's and the voxel's compliance can be seen for the thinnest structure. This is caused by the discretization with only three voxel elements across the wall thickness. This coarse discretization leads to an artificial stiffening of the structure.

### 6.6 Mechanical interpretation of the optimized designs

In Fig. 18 the cross sections of the optimized sheet metal with a wall thickness of 1.875 mm is displayed. It can be seen that the sheet metal moves towards the upper and lower design space boundary at the clamped end in order to bear the bending moment around  $y$  with the lowest possible reaction forces. At the back end the shell forms a U-channel, while it becomes an M-channel at the front end in order to reach an equal stiffness across the whole width of the loading edge. Additionally there is a bead at the middle of the loading edge, which supports the middle of the loading edge at the symmetry plane to take bending moments around  $x$ . This bending moment is also absorbed by the fold going along the outer section of the loading edge towards the clamped end.

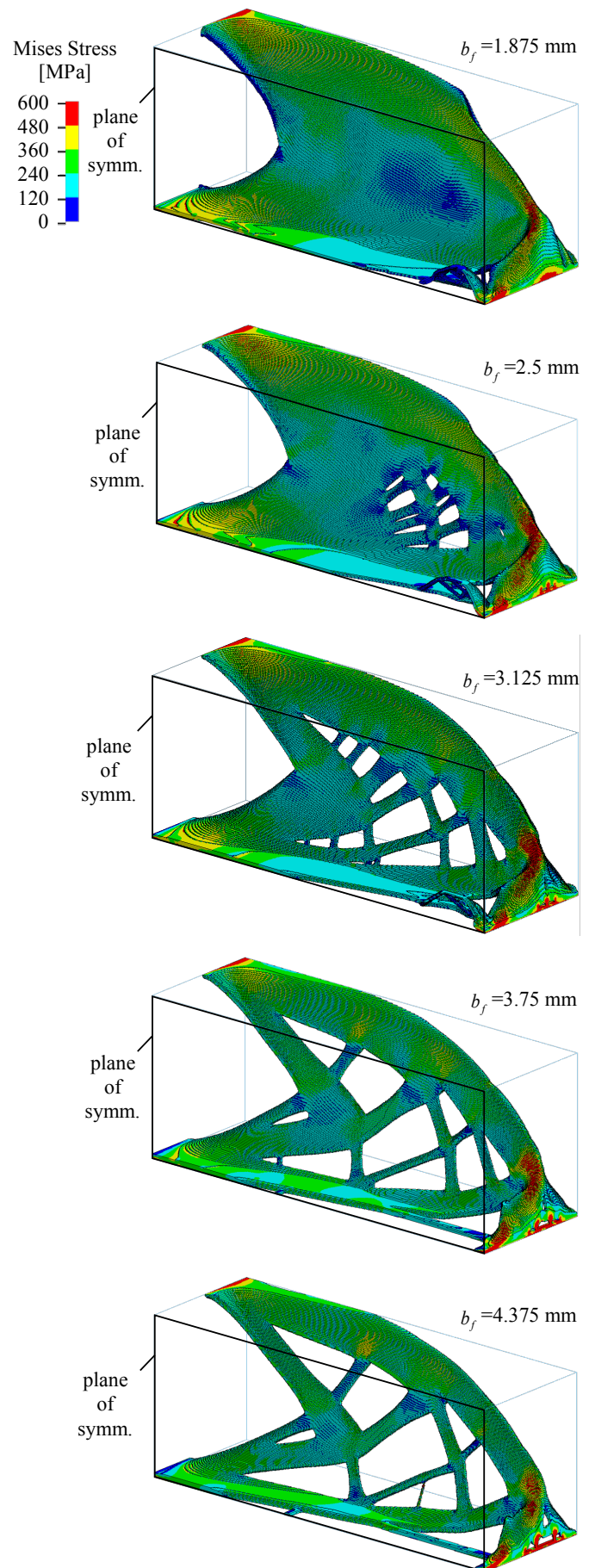
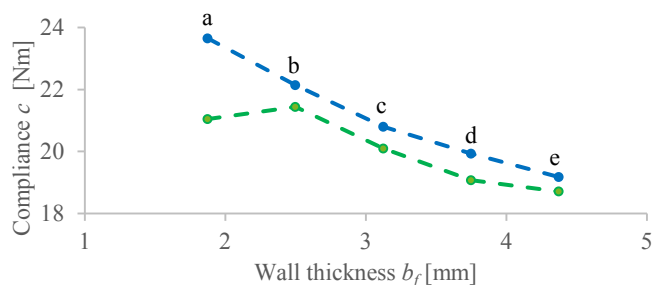
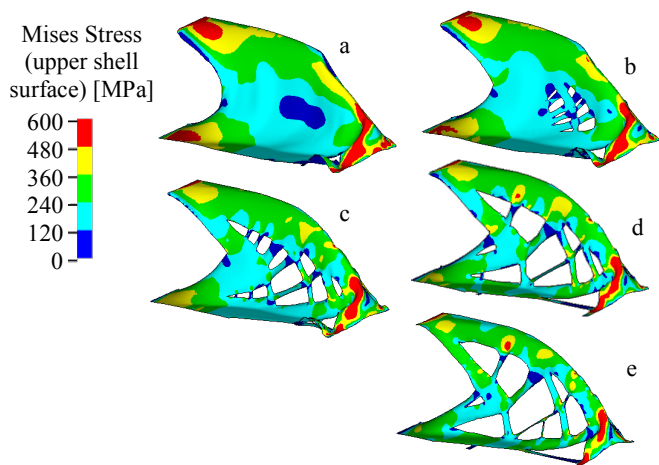


Fig. 15 Optimized Cantilever Beam with increasing wall thickness – half model



**Fig. 16** Structural performance of optimized structures from Fig. 15 calculated with voxel elements (green) and remodeled shells (blue)



**Fig. 17** FE-results of remodeled shells, a-e correspond with Fig. 16

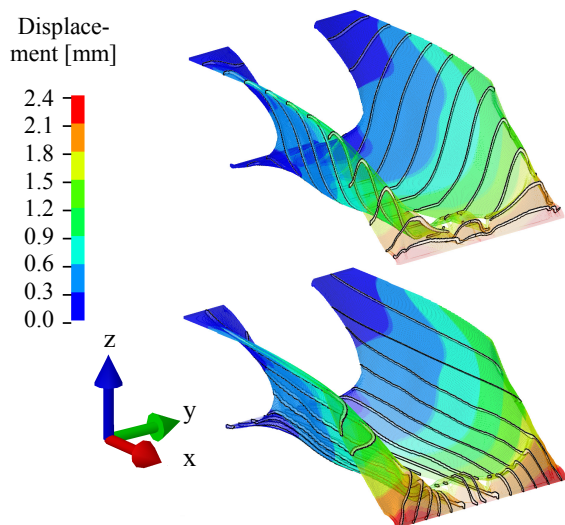


**Fig. 18** Cross sections of the thinnest optimized design

### 6.7 Cantilever beam with point load – variation of stamping direction

In order to show the effect of a changing punch direction, the load case was modified. Now a load of  $F=10$  kN is applied at an eccentric point on the front surface of the design space as to be seen in Fig. 19. No non-design space is defined. All other optimization parameter remain the same.

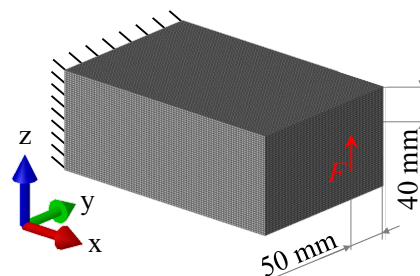


**Fig. 19** Load case for different punch directions

Fig. 20 shows the optimization results. In Fig. 20a the result without manufacturing constraint is shown. This optimized density distribution is used as initial design for the optimizations with manufacturing constraint in order to start with a structure, that connects the clamped end of the design space and the loading point.

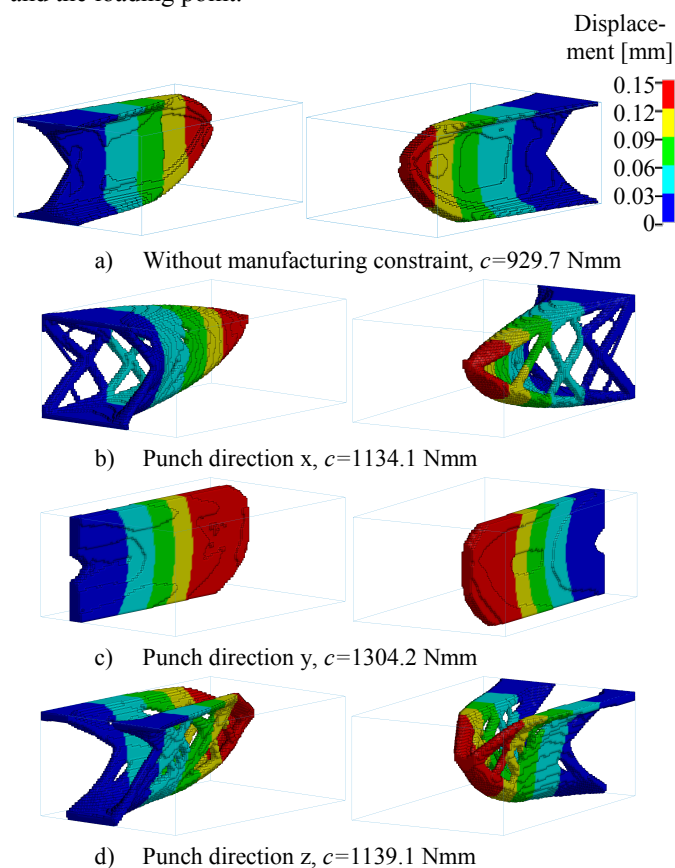
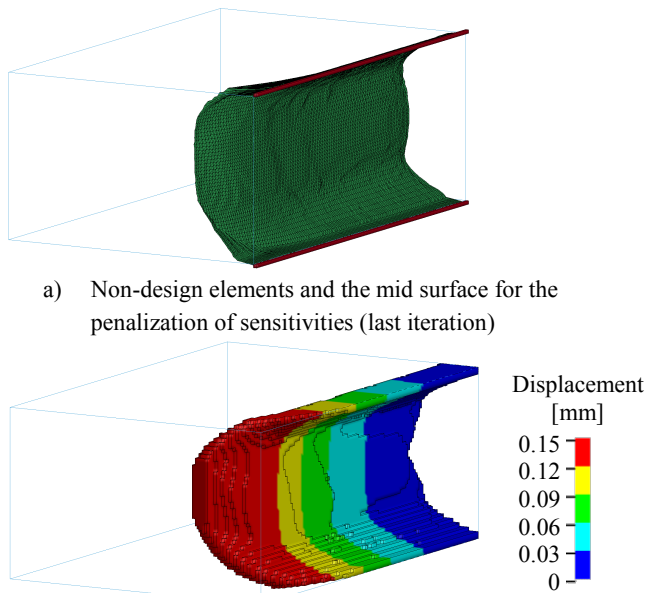


**Fig. 20** Optimized Cantilever Beam for different punch directions

As expected, the optimization without manufacturing constraint results in the best compliance. Depending on the punch direction completely different optimized structures develop. Here punch directions x and z are far better than punch direction y. For Fig. 20c the initial design, the used design space and the load case are nearly symmetric, therefore also the sensitivities to both sides of the shell are symmetric and consequently the mid surface does not change during the optimization.

In order to prescribe a preferred camber direction for this punch direction, one element row of non-design elements is added at the boundary of the design space (red elements in Fig. 21a). They are not connected to the design elements, so they do not

contribute the structure's stiffness. They ensure, that the mid surface (shown as green shell elements in Fig. 21a) for the penalization of sensitivities is curved towards the positive y-direction at the upper and lower end of the design space. Therefore the sensitivities on this side of the shell are less penalized and the upper and lower end of the mid surface can move towards the positive y-direction. Consequently the improved shell structure in Fig. 21b has a 14 % lower compliance.



a) Non-design elements and the mid surface for the penalization of sensitivities (last iteration)  
b) Optimized Cantilever Beam,  $c=1104.5$  Nmm  
**Fig. 21** Punch direction y with prescribed camber direction

The compliance values of all punch directions are nearly the same. In a practical design process one of these three results will be selected by manufacturing criteria.

## 7 Example 2 – Quadratic Plate

As a further example a quadratic plate is optimized (adapted from Bletzinger and Ramm 2014). The design space cuboid ( $200 \cdot 200 \cdot 20$  mm) is discretized with voxels of 0.5 mm edge length. The objective function is the compliance, the volume fraction is constrained to 7.5%. Fig. 22 shows the load case and the design space. A force of  $F=4000$  N is applied at the center of the design space. Along the small faces the structure is clamped near each corner at a length of 50 mm. The material is steel ( $E_0 = 210$  GPa,  $\nu = 0.3$ ). A sensitivity filter with the radius of  $r = (1.7$  element edge lengths) and a penalty exponent  $s = 3$  are used. Only a quarter of the design space is used during the optimization using the symmetry planes perpendicular to x and y.

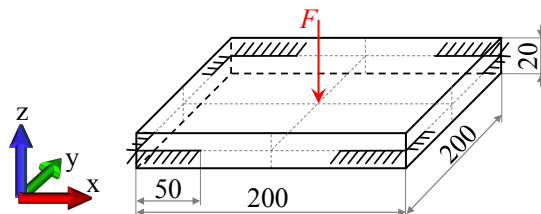


**Fig. 22** Quadratic Plate – load case and design space, distances in mm

### 7.1 Results without manufacturing constraint

Without the manufacturing constraint the element densities were initialized uniformly. 500 iterations were performed, resulting in a compliance of 321.4 Nmm for the full structure (see Fig. 23). The wall-clock time was approximately 20 hours. Most structural elements are located at the upper and lower boundary of the design space.

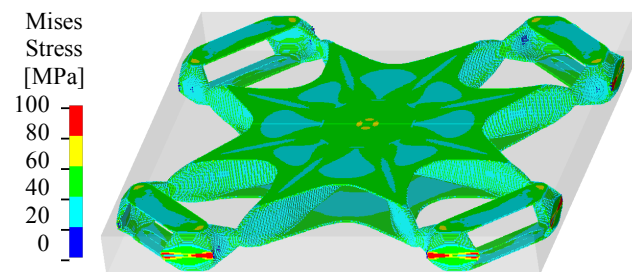


**Fig. 23** Optimized Quadratic Plate without manufacturing constraint (black&white design)

### 7.2 Results with manufacturing constraint

The punch direction was chosen as z, the desired wall thickness is 4 element edge lengths, i.e. 2 mm. If the design elements were initialized with a uniform density distribution, a symmetric design regarding the z-direction develops. For a thin walled structure this is a flat sheet. In order to avoid this symmetry, the design space is initialized asymmetrically (see Fig. 24). After 605 Iterations and a calculation time of 30 hours a compliance of 544.7 Nmm is achieved, which is nearly 70 % worse than the optimized design without manufacturing constraint.

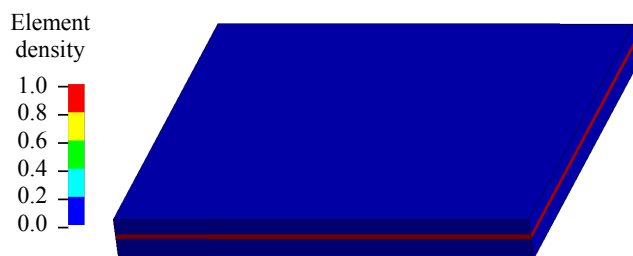


**Fig. 24** Initial density distribution of the Quadratic Plate with manufacturing constraint

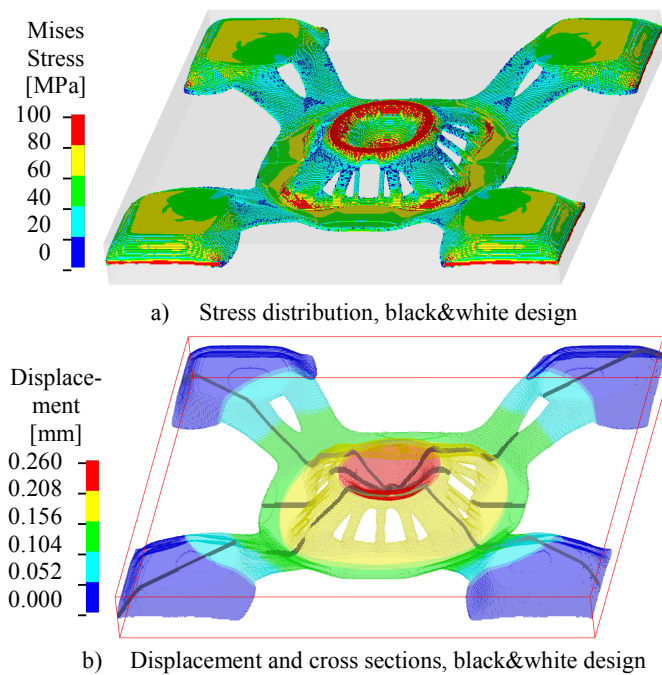


**Fig. 25** Optimized Quadratic Plate with manufacturing constraint

## 8 Conclusion

The presented approach is a powerful possibility for finding shell structures manufactured by deep drawing. The manufacturing constraints can be fulfilled, but the computational cost is an increased number of iterations and a decline of the objective function of the optimized design due to the restricted design freedom.

In the examples it has been shown that considering topology optimization for shell structures can be useful, because cut outs can be used to improve the performance of the component, at least for compliance minimization with a single load case.

For very thin shells the discretization has to be very fine in order to reach realistic results. Therefore the computational effort increases with a thinning of the shell.

Besides the shown application examples, the manufacturing constraints for the topology optimization of deep drawable sheet metals has been tested for several structures, also with multiple load cases. The results are promising, but we have to note that the gradient based optimization method will find most probably only local optima.

Further research activities will focus on the improvement of the computational efficiency (e.g. adaptive change of objective wall thickness to perform optimization in one loop), multishell structures, buckling constraints and automation of the conversion to a surface model in order to perform a following shape optimization. Also the deep drawing simulation will be implemented in the optimization to ensure the formability of the sheet metal without tearings or wrinkles.

## References

- Allaire, G.; Jouve, F.; Michailidis, G. 2013: Casting constraints in structural optimization via level-set method, *Proc. of 10th World Congress on Structural and Multidisciplinary Optimization*, Orlando, USA
- Ansola R.; Canales, J.; Tarrago, J.A.; Rasmussen, J. 2002: On simultaneous shape and material layout optimization of shell structures, *Struct Multidisc Optim* 24, 175-184
- Bendsøe, M.P. 1989: Optimal shape design as a material distribution problem, *Struct Optim* 1, 193-202
- Bertsch, C.; Cislino, A.P.; Langer, S.; Reese, S. 2008: Topology Optimization of 3D Elastic Structures Using Boundary Elements, *Proc Appl Math Mech* 8, 10771-10772
- Bletzinger, K.U.; Ramm, E. 2014: A consistent frame for sensitivity filtering and the vertex assigned morphing of optimal shape, *Struct Multidisc Optim* 49, 873-895
- Boljanovic, V. 2014: Sheet Metal Forming Processes and Die Design, South Norwalk: Industrial Press
- Dienemann, R.; Schumacher, A.; Fiebig, S. 2016: Topology and Shape Optimization of Sheet Metals with integrated Deep-Drawing-Simulation, *Proc. of 12th World Conference on Computational Mechanics*, Seoul, Korea
- Falkenberg, P.; Franke, T.; Fiebig, S.; Vietor, T. 2015: Consideration of adhesive joints for a multi-material topology optimization approach, *20th International Conference on Composite Materials*, Copenhagen, Denmark
- Fiebig, S.; Sellschopp, J.; Manz, H.; Vietor, T.; Axmann, K.; Schumacher, A. 2015: Future challenges for topology optimization for the usage in automotive lightweight design technologies, *Proc. of 11th World Congress on Structural and Multidisciplinary Optimization*, Sydney, Australia
- Fleury, C. 1989: CONLIN: an efficient dual optimizer based on convex approximation concepts, *Struct. Optim.* 1, 81-89
- Franke, T.; Vietor, T.; Fiebig, S.; Horstmann, G.M. 2015: Robust and production-oriented topology optimization of cast parts including manufacturing restrictions and process simulation, *NAFEMS seminar Optimierung und Robust Design*, Wiesbaden, Germany
- Guest, J.; Zhu, M. 2012: Casting and Milling Restrictions in Topology Optimization via Projection-Based Algorithms, *Proceedings of the ASME 2012 International Design Engineering Technical Conference & Computers and Information in Engineering Conference*, Chicago, IL, USA
- Harzheim, L.; Graf, G. 2006: A review of optimization of cast parts using topology optimization II – Topology optimization with manufacturing constraints, *Struct Multidisc Optim* 31, 388-399
- Hassani, B.; Tavakkoli S.M.; Ghasemnejad, H. 2013: Simultaneous shape and topology optimization of shell structures, *Struct Multidisc Optim* 48, 221-233
- Le, C.; Norato, J.; Bruns, Z.; Ha, C.; Tortorelli, D. 2010: Stress-based topology optimization for continua, *Struct Multidisc Optim* 41, 605-620
- Lochner-Aldinger, I.; Schumacher, A. 2014: Homogenization method, In: Adriaenssens, S.; Block, P.; Veenendaal, D.; Williams, C. *Shell Structures for Architecture – Form Finding and Optimization*, New York: Routledge
- Sigmund, O.; Petersson, J. 1998: Numerical instabilities in topology optimization: A survey on procedures dealing with checkerboards, mesh-dependencies and local minima, *Struct Multidisc Optim* 16, 68-75

Sigmund, O.; Aage, N.; Andreassen, E. 2015: On the optimality of Michell structures, *Proc. of 11th World Congress on Structural and Multidisciplinary Optimization*, Sydney, Australia

Svanberg, K. 1987: The method of moving asymptotes – a new method for structural optimization. *Int. J. Numer. Meth. Engrg.* 24, 359–373

Xia, Q.; Shi, T.; Wang, M.Y.; Liu, S. 2009: A level set based method for the optimization of cast part, *Struct Multidisc Optim* 41, 735-747

Zhou, M.; Fleury, F.; Patten, S.; Stannard, N.; Mylett, D.; Gardner, S. 2011: Topology Optimization - Practical Aspects for Industrial Applications, *Proc. of 9th World Congress on Structural and Multidisciplinary Optimization*, Shizuoka, Japan